



Research article

Development of low-cost and high-efficiency solar modules based on perovskite solar cells for large-scale applications

Muhammad Shoaib Hanif^a, Irfan Qasim^{b,*}, Muhammad Imran Malik^c,
Muhammad Farooq Nasir^a, Owais Ahmad^d, Asim Rashid^e

^a Materials Research Laboratory, Department of Physics (FEAS), Riphah International University, Islamabad, 44000, Pakistan

^b Department of Physics, Faculty of Sciences, Rawalpindi Women University, 6th Road, Satellite Town, 46300 Rawalpindi, Pakistan

^c School of Electrical Engineering and Computer Science (SECS), National University of Sciences and Technology (NUST), Islamabad 44000, Pakistan

^d Department of Physics, Macquarie university, Sydney, Macquarie Park NSW 2109, Australia

^e Technical Developer Renewables, Fortum corporation, POB 100, FI-00048 Keilalahdentie 2-4, Finland

ARTICLE INFO

Keywords:

Optoelectronic
Mobilities
Renewable
Perovskite
Quantum efficiency

ABSTRACT

Solar energy has emerged as a viable and competitive renewable resource due to its abundance and cost-effectiveness. To meet the global energy demands, there is a growing need for efficient devices with unique compositions. In this study, we designed and analyzed a perovskite solar cell (PSC) incorporating methylammonium tin iodide ($\text{CH}_3\text{NH}_3\text{SnI}_3$) as the active optical absorber material, tin iodide (SnO_2) as the electron transport layer (ETL), and copper thiocyanate (CuSCN) as the hole transport layer (HTL) using SCAPS-1D software for numerical investigations. Subsequently, the optimized outcomes were implemented in the PVSyst software package to derive the characteristics of a solar module based on the proposed novel solar cell composition. The objective of our research was to enhance the stability of solar cell for use in solar module. This was achieved by optimizing the thicknesses of the compositional layers which resulted in the enhancement of excess electron and hole mobilities and a reduction in defect densities, thereby leading to an improvement in the device performance. The optimization of excess electron and hole mobilities, as well as defect densities, was conducted to improve the device performance. SCAPS calculations indicated that the perovskite absorber layer ($\text{CH}_3\text{NH}_3\text{SnI}_3$) may achieve the best possible performance with a maximum optimized thickness of 3.2 μm . The optimized thickness value for CuSCN -HTL and SnO_2 -ETL were found to be 0.07 μm and 0.05 μm respectively resulting in a maximum power conversion efficiency (PCE) of 23.57%. Variations in open circuit voltage (V_{oc}), short circuit current (J_{sc}), fill factor (FF %), and quantum efficiency (QE) associated with the optimized thickness values of all layers in the ITO/ SnO_2 / $\text{CH}_3\text{NH}_3\text{SnI}_3$ / CuSCN /Mo composition were critically analyzed. The use of these input parameters resulted in power creation of 557.4 W for a module consisting of 72 cells with an annual performance ratio of 80.3%. These recent investigations are expected to be effective in the design and fabrication of eco-friendly and high-performance solar cells in terms of efficiency.

* Corresponding author.

E-mail address: dr.irfanqasim@gmail.com (I. Qasim).

<https://doi.org/10.1016/j.heliyon.2024.e25703>

Received 13 July 2023; Received in revised form 4 January 2024; Accepted 31 January 2024

Available online 8 February 2024

2405-8440/© 2024 The Authors. Published by Elsevier Ltd. This is an open access article under the CC BY-NC-ND license (<http://creativecommons.org/licenses/by-nc-nd/4.0/>).

1. Introduction

The utilization of energy resources in our day-to-day lives has significantly increased in line with the growth of modern civilizations. To keep pace with the demands of modern development, the need for efficient and sustainable energy sources has become even more pressing. Among the emerging photovoltaic technologies, perovskite absorber material-based organic and inorganic solar cells have made significant strides in recent times. By analyzing the progress chart of different classifications of solar cells over time, we can observe the remarkable advancement of perovskite absorber material-based solar cells [1–3]. Perovskite-based photovoltaic technology has emerged as a promising alternative to conventional solar cell technologies in the last decade. This is due to its ability to attain high values of critical parameters such as short-circuit current density (J_{sc}), open-circuit voltage (V_{oc}), quantum efficiency (QE) and power conversion efficiency (PCE).

The unique crystal structure of perovskite materials allows for high charge carrier mobility and a wide range of tunable optical and electronic properties. These characteristics have contributed to the impressive performance of perovskite solar cells (PSCs) in recent years, with PCEs exceeding 25%. One of the most significant advantages of PSCs is their ability to be manufactured through low-cost and scalable solution-based methods. This makes them an attractive option for large-scale deployment in the future. Overall, the emergence of perovskite-based photovoltaic technology has ushered in a new era of innovation in the field of solar energy. With continued research and development, PSCs have the potential to play a crucial role in meeting the world's growing energy needs sustainably [4,5]. Numerous researchers have employed a variety of simulation software, including SCAPS, to explore the physical, mechanical, optical, and electrical properties of perovskite compounds as absorber layers in photovoltaic technology, owing to their exceptional performance in these areas [6,7]. The utilization of perovskite material in both organic and inorganic halide-based solar cells signifies its role as an active optical absorber layer, the properties of which are pivotal for overall performance [8,9]. Instability and a reduction in the lifespan of perovskite material, along with the hazardous effects associated with lead (Pb), raise substantial concerns regarding its future use, despite its desirable efficiency [10–12]. Inorganic halide perovskites like tin, silver, and copper, with energy band gaps exceeding 2 eV, are deemed less favorable for modern photovoltaic technology. Additionally, the low open-circuit voltage values associated with antimony (Sb) and Sn^{2+} cations, as well as the poor charge transport capability of bismuth (Bi), make them less attractive due to their instability. Nevertheless, a comparison with silicon-based solar cells reveals that perovskite-based solar cells have demonstrated a remarkable increase in power conversion efficiency (PCE) over the past twelve years, soaring from 3% to over 20%. This progress serves as compelling evidence of the potential of perovskite solar cells compared to other classifications [13–15]. However, the limited availability of certain hole transport materials, such as Spiro-OMETAD, has hindered the use of perovskite absorber material in the global market, leading to reduced durability and increased overall device cost [16,17]. Researchers have made significant progress in the use of perovskite solar cells by achieving the desired values of current density, electron and hole mobility, absorption coefficient, and tunable bandgap of perovskite compounds. Despite these achievements, perovskite solar cells face serious challenges due to the toxic nature of lead, overall performance instability with hysteresis, and high cost. Therefore, it is imperative to optimize all associated parameters of perovskite solar cells to attain desirable performance at a reasonable cost. This endeavor will contribute to the development of more efficient and cost-effective perovskite solar cells, potentially making a substantial impact on the renewable energy sector.

A range of organo-halide perovskite compounds, such as $\text{CH}_3\text{NH}_3\text{YZ}_3$ ($Y=\text{Sn, Pb, Ge}$) ($Z = \text{Cl, Br, I}$), are available for optimizing various associated parameters while reducing toxicity levels and enhancing overall device stability [18]. Hui-Jing Du et al. conducted a study on tin-based perovskite solar cells, specifically $\text{CH}_3\text{NH}_3\text{SnI}_3$, using simulations. The results revealed an open-circuit voltage of 0.92V, a short-circuit current density of 31.59 mA/cm², a fill factor of 79.9%, and a power conversion efficiency of 23.36%. The study found that Sn-based perovskite solar cells are more efficient compared to Pb-based ones, as Sn is free from toxicity, and Sn^{+2} cations are highly stable. Overall, this research highlights the potential of Sn-based perovskite solar cells as a promising alternative to Pb-based ones, due to their improved stability and efficiency, while also addressing concerns over the toxicity of lead [19–21].

In our current research, we have conducted a study on perovskite solar cells based on $\text{CH}_3\text{NH}_3\text{SnI}_3$ as the active absorber, under varying applied conditions. We have optimized the thicknesses, metal work functions, defects and interface defect densities of the absorber layer, HTL, and ETL while also considering temperature variations. Our study has focused on understanding the impact of defect density, interface defects, charge carrier generation, and recombination, as well as the energy band gaps on the overall performance of the device. The obtained parameters were inserted into the well-established PVSyst software to acquire solar module characteristics in terms of achieved power and annual performance ratio. In this research, our main focus was on optimizing all associated parameters to achieve a high power conversion efficiency (PCE) of a single solar cell while also keeping the manufacturing cost low. Our ultimate goal is to extend these optimized parameters to create a solar module that is both efficient and cost-effective on a commercial scale. By doing so, we hope to contribute to the development of more advanced and economically viable perovskite solar cells and modules.

2. Numerical simulations and Methodology

The modeling and optimization of perovskite solar cells can be achieved by using SCAPS 1-D software. The software was developed by the University of Ghent in Belgium and incorporates algorithms based on three versatile partial differential equations (PDEs). Equation (1) delineates the Poisson's relation governing electrons and holes. It is seamlessly incorporated in the simulation package in standard form as represented below;

$$\frac{\partial^2 \Psi}{\partial x^2} = -\frac{\partial E}{\partial x} = -\frac{\rho}{\epsilon_s} = -\frac{q}{\epsilon_s} [p - n + N_d^+ + N_a^- \pm N_{def}] \quad (1)$$

Where Ψ corresponds to electrostatic potential, E represents the electric field, ϵ_s as relative permittivity (static), q denotes charge, e as electron, n also stands for electron, N_d^+ represents donor's density, N_a^- denotes acceptor's density along with N_{def} as defect density associated with donor and acceptor. Equations (2) and (3) together demonstrate the continuity equations for electrons as well as the holes are represented as below;

$$-\frac{\partial j_p}{\partial x} + G - U_p(n, p) = 0 \quad (2)$$

And

$$-\frac{\partial j_n}{\partial x} + G - U_n(n, p) = 0 \quad (3)$$

Where J_p corresponds to current density associated with holes, J_n represents current density associated with electrons, $U_n(n, P)$ stands for recombination rates associated with electrons, $U_p(n, P)$ signifies recombination rates associated with holes, G denotes generation rate associated with carrier (electrons and holes). Expressions (4) and (5) portray the current density for both electrons and holes, as articulated below;

$$j_p = qm\mu_p E - qD_p \frac{\partial p}{\partial x} \quad (4)$$

And

$$j_n = qm\mu_n E - qD_n \frac{\partial n}{\partial x} \quad (5)$$

Where q corresponds to charge, μ_p represents electron mobility, μ_n stands for hole mobility, D_p signifies the diffusion coefficient associated with holes, D_n represents the diffusion coefficient associated with electrons. The SCAPS 1-D simulation software utilizes above set of equations and enables the calculation of various parameters of a solar cell, including current density (J_{sc}), efficiency, fill factor, and open circuit voltage (V_{oc}), across a range of thicknesses and temperatures. This simulation is not restricted to a light environment but can also be conducted in a dark environment, and can account for diverse temperature conditions [22–24].

The designed model and the composition framework aligned with the simulated perovskite solar cell ITO/SnO₂/CH₃NH₃SnI₃/CuSCN/Mo is manifested in figure-1. In this composition, the work functions of front as well as the back contact layers are 4.62 for ITO material and 4.95 for Mo.

The thickness of each layer was optimized to achieve maximum performance. The interfacial defect layers SnO₂/CH₃NH₃SnI₃-Perovskite and CH₃NH₃SnI₃-Perovskite/Mo were considered for simulation, along with their associated parameters [25–27]. The input parameters were obtained from the literature and verified through density functional theory. The optimization process involved varying the thickness of each layer while keeping the thickness of the corresponding two layers constant. Initially, the thickness of the SnO₂ layer was varied from 0.040 nm to 0.060 nm while keeping the thickness of the CH₃NH₃SnI₃-Perovskite and CuSCN layers fixed, and the maximum power conversion efficiency (PCE) was observed for this layer. Next, the thickness of the CH₃NH₃SnI₃-Perovskite layer was varied from 2.68 μ m to 3.30 μ m while keeping the thickness of the SnO₂ and CuSCN layers constant, and the maximum PCE was observed for this layer. Similarly, by keeping the thickness of the CH₃NH₃SnI₃-Perovskite and SnO₂ layers constant, the thickness



Fig. 1. Structure of proposed solar cell composition.

of the CuSCN layer was varied between 0.05 μm and 0.08 μm , and the maximum PCE was observed for this layer [28,29]. Finally, we simulated the optimized results for the ITO/SnO₂/CH₃NH₃SnI₃/Mo solar cell structure using the optimized values of all layers [30,31]. The steps involved in this procedure were employed for both the optimization of composition and the evaluation of associated parameters, as illustrated in figure-2.

The results obtained from the optimized single solar cell were then inserted into the PVSyst software package for module analysis simulations. PVSyst is a software tool used to design, simulate, and analyze the performance of solar photovoltaic systems. The software utilizes input data such as system configuration, location-specific weather conditions, and module specifications, to create a model of the solar PV system. With this model, PVSyst can simulate the system's energy output and provide information such as annual energy production, system efficiency, and capacity factor. The software also accounts for shading analysis, inverter efficiency, and other system losses to provide a realistic representation of its performance. Moreover, PVSyst boasts a comprehensive database of meteorological data for over 30,000 locations worldwide, enabling accurate simulation of solar energy production in various weather conditions. Additionally, the software provides detailed financial analysis, encompassing costs, payback periods, and return on investment calculations, which are valuable for assessing the economic feasibility of a solar PV system. In summary, PVSyst is a powerful tool for optimizing the design and performance of solar PV systems.

3. Results and discussion

3.1. Optimized performance of proposed solar cell composition using SCAPS-1D

The energy band alignment of a solar cell, comprising multiple layers that collaborate to convert sunlight into electrical energy is shown in the figure-3. The front contact layer is made of indium tin oxide (ITO) with a work function of 4.62 eV. Following this layer is the electron transport layer, composed of tin oxide (SnO₂) with an optimized thickness of 0.05 μm . This layer is responsible for transporting electrons from the absorber layer to the front contact layer. The absorber layer is fabricated from a hybrid organic-inorganic perovskite material, CH₃NH₃SnI₃, with a thickness of 3.2 μm . This layer absorbs the sunlight and converts it into electrons and holes, which are subsequently separated and collected by the electron and hole transport layers respectively. The hole transport layer is made of copper thiocyanate (CuSCN) with an optimized thickness of 0.07 μm , gathers the holes generated in the absorber layer and transports them to the back contact layer. The back contact layer is made of molybdenum (Mo) with a work function of 4.95 eV. This layer collects the electrons, thus completing the circuit and enabling the utilization of the generated electrical energy.

The energy band alignment of the solar cell shows that the absorption of photons by the perovskite material leads to the creation of an electron-hole pairs, which are separated by the built-in potential of the absorber layer. The electrons are transported to the front contact layer through the electron transport layer, while the holes are transported to the back contact layer through the hole transport layer. The energy difference between the top of the valence band of the absorber layer and the work function of the back contact layer determines the open circuit voltage of the solar cell. Overall, the optimized layer thicknesses and work functions of the different layers contribute to the high power conversion efficiency of the solar cell.

By making minor adjustments to the optimized values of the integrated layers, the overall efficiency of the device can be reduced, which is an undesirable outcome. Figure-4 illustrates the optimized band diagram of the associated energy for the CH₃NH₃SnI₃-based solar cell appliance, representing the most favorable layout for maximum output. Through the fine-tuning of the band gap values for CuSCN, CH₃NH₃SnI₃, and SnO₂, we have successfully attained the optimal band gap values of 3.4 eV for CuSCN, 1.35eV for CH₃NH₃SnI₃, and 3.6eV for SnO₂. The mobility of charge carriers has a significant impact on the overall performance of the device. Increasing the mobilities of electrons and holes enhances the power conversion efficiency (PCE) of the CH₃NH₃SnI₃ perovskite absorber. However, an increase in mobility corresponds to an increase in the value of J_{sc} and a reduction in V_{oc}, resulting in a decrease



Fig. 2. Stepwise simulation process in SCAPS-1D.

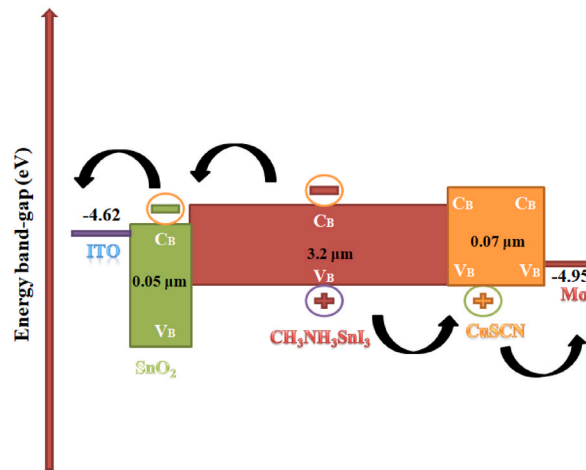


Fig. 3. Energy band alignment diagram of the proposed solar cell.

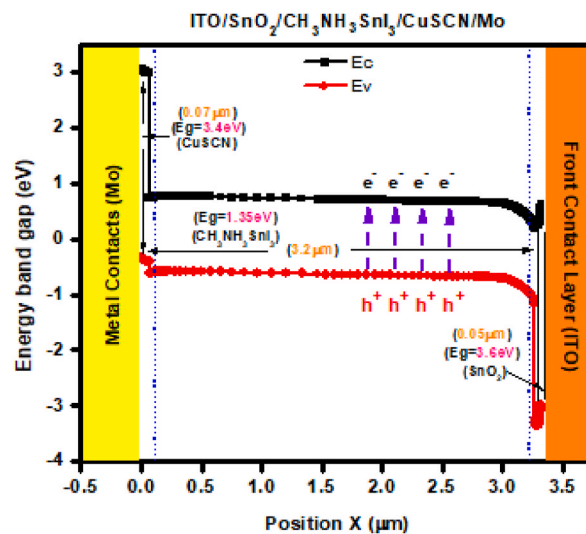


Fig. 4. Optimized energy band diagram of the $\text{CH}_3\text{NH}_3\text{SnI}_3$ -based solar cell.

in PCE. Additionally, the Fermi energy of the n-type material, SnO_2 , should be lower than that of the p-type material, CuSCN .

Quantum efficiency (QE) versus wavelength plot for a solar cell is an important tool for evaluating its performance. The QE plot shows the percentage of photons that are absorbed by the solar cell as a function of wavelength. It provides information about the ability of the solar cell to convert different wavelengths of light into electrical energy. Typically, the QE plot exhibits a peak at a certain wavelength, corresponding to the maximum absorption of light by the solar cell. This peak is associated with the band gap of the semiconductor material used in the solar cell. The bandgap determines the minimum energy required for a photon to be absorbed and create an electron-hole pair, which can be collected as electrical current. In general, a high QE value signifies a more efficient solar cell, indicating that a higher percentage of incident photons are being absorbed and converted into electrical energy. A QE plot serves as a valuable tool for comparing the performance of diverse solar cell materials and designs, as well as for pinpointing areas where solar cell efficiency can be enhanced. Figure-5 displays the effect of wavelength on quantum efficiency. The quantum efficiency (QE) trend is observable across three wavelength regions: ultraviolet (UV), visible, and infrared (IR), spanning from 300 nm to over 900 nm. Comparatively small absorption is noted in the ultraviolet region. However, maximum absorption occurs in the visible region, specifically within the range of 400–700 nm. The near-infrared region also exhibits favorable absorption. The maximum value of quantum efficiency (QE) corresponds to the efficient absorption of sunlight. In contrast, the quantum efficiency descends abruptly in the far-infrared region, beyond which the overall device performance diminishes in accordance with the equation.

Additionally, as wavelength (λ) increases, energy (E) decreases, resulting in the perovskite-based solar cell's inability to absorb light.

The J-V characteristics of a solar cell can be used to determine the cell's efficiency, quantifying how effectively the cell transforms

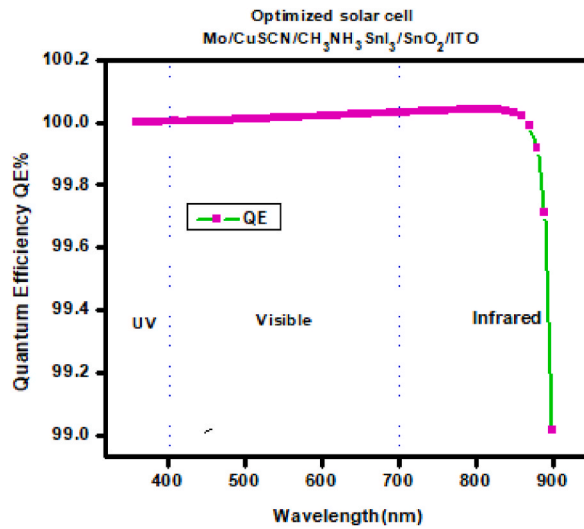


Fig. 5. Quantum Efficiency (QE) in relation with the wavelength (λ) of incident sunlight.

sunlight into electrical energy. The J-V (current-voltage) characteristics of a solar cell represent the relationship between the cell's output current and voltage under varying conditions of illumination and load resistance. The J-V curve is a graphical representation of the electrical behavior of the solar cell, and it is an important tool for evaluating the performance of the cell. The J-V characteristic curve of the CH₃NH₃SnI₃-perovskite based solar cell is presented in figure-6. The measurements were taken for the optimized thicknesses of the SnO₂/CH₃NH₃SnI₃/CuSCN layers of the cell, revealing several associated parameters, including an open-circuit voltage (V_{oc}) of 0.92061 V, a short-circuit current density (J_{sc}) of 34.38459 mA/cm², a Fill Factor (FF) of 74.4616%, and a power conversion efficiency of 23.570%.

It is important to note that negative values of the total current density (J_{sc}) indicate that the current is flowing from the device to the system, with the amount of current added to the system equal to the amount of current removed from the device. The observed values of J_{sc} , V_{oc} , FF, and efficiency demonstrate the favorable performance of the CH₃NH₃SnI₃-perovskite based solar cell. The optimized thicknesses of the integrated layers play a pivotal role in achieving these positive results. Negative values of current density (J_{sc}) on the vertical axis of the J-V characteristic curve of a solar cell indicate that the current is flowing from the device to the system. This means that the amount of current added to the system equals the amount of current removed from the device.

The J-V characteristic curves, as depicted in Figure-7, provide valuable insights into the influence of temperature variations on the total current density of the ITO/SnO₂/CH₃NH₃SnI₃/CuSCN/Mo perovskite-based solar cell. It is noteworthy that these curves represent a range of temperatures. Interestingly, the results indicate that as the temperature increases from 300 K to 340 K, there is no significant change in the current density (J_{sc}) for voltage values ranging from 0.0 V to 0.6 V. This observation suggests that the performance of the perovskite-based solar cell is relatively stable within the given temperature range. One plausible explanation is that the temperature

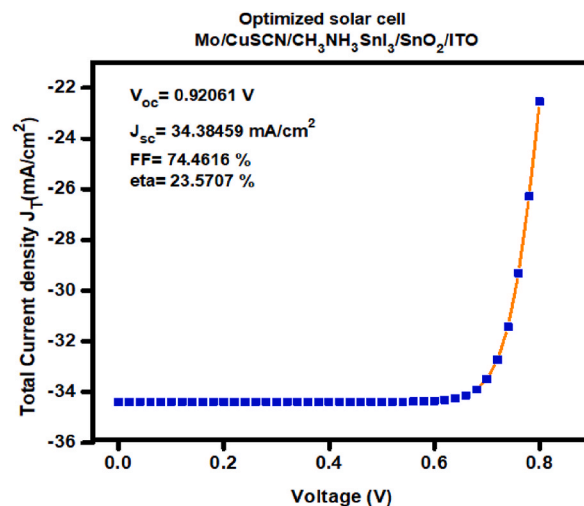


Fig. 6. J-V Characteristic curve for optimized CH₃NH₃SnI₃-incorporated solar cell.

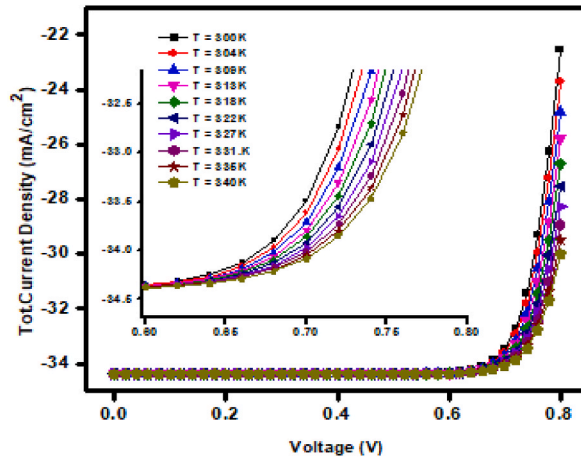


Fig. 7. Temperature dependent J-V Characteristic of proposed solar cell.

increase enhances carrier mobility, consequently resulting in a higher open-circuit voltage. Additionally, an increase in temperature can also lead to a reduction in the recombination rate of charge carriers, further contributing to an increase in open circuit voltage.

The process of carrier generation is a critical step in the operation of a solar cell. When photons from the sun are absorbed by the material in the solar cell, they transfer their energy to the electrons in the material, leading to the creation of charge carriers. These charge carriers are then used to produce an electrical current that can be harnessed for practical purposes. Consequently, the efficiency of a solar cell is directly dependent on the rate at which it can generate charge carriers. It is, therefore, imperative to comprehend and optimize the rate at which carriers are generated within a solar cell. By improving the generation rate of carriers, we can increase the overall efficiency of the solar cell, which is critical for the widespread adoption of solar energy. The carrier generation rate in a solar cell is primarily determined by the absorption coefficient of the semiconductor material and the intensity of incident light. When light shines on a semiconductor material, photons with energy greater than or equal to the bandgap energy of the material are absorbed, creating electron-hole pairs (charge carriers). The absorption coefficient describes the likelihood of this absorption phenomenon, and is a function of the material properties and the wavelength of the incident light. Figure-8 displays the variation in the generation rate of charge carriers with depth within the composition. The diffusion length of the device, which includes the HTL, absorber, and ETL, is also shown in the plot. Notably, the data reveals that initially, up to a thickness value of 2.7 μm , no generation of charge carriers is observed when light enters the surface. However, from 2.7 μm to 3.3 μm , there is a significant increase in carrier generation. The peak generation rate (Geh) of $1.40 \times 10^{22} \text{ cm}^{-3}\cdot\text{s}$ is observed at a depth of 3.35 μm .

In any solar cell, recombination is a significant factor that limits device performance. Recombination occurs when the photo generated electrons and holes (carriers) recombine before they can reach the respective electrodes, resulting in a loss of energy and a decrease in the overall efficiency of the solar cell. There are several types of recombination mechanisms that can occur in a perovskite solar cell, including radiative recombination, non-radiative recombination, trap-assisted recombination, surface recombination, and bulk recombination. To improve the performance of perovskite solar cell, reducing the recombination rate is critical. Strategies to reduce recombination include passivation of the surfaces and defects in the perovskite material, optimizing the thickness of the perovskite layer, and improving the quality of the interfaces between the different layers of the solar cell. Figure-9 shows the variation

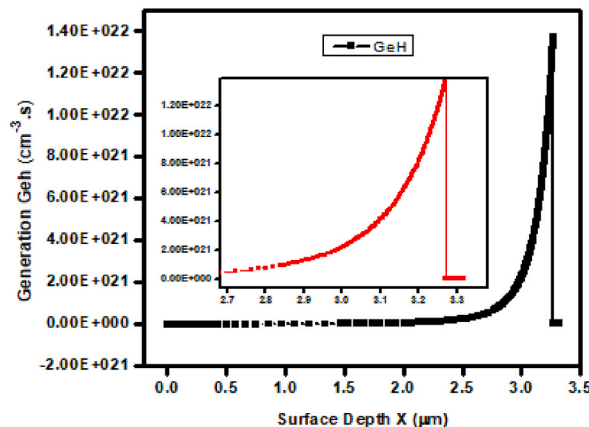


Fig. 8. Generation rates versus thickness of optimized solar cell.

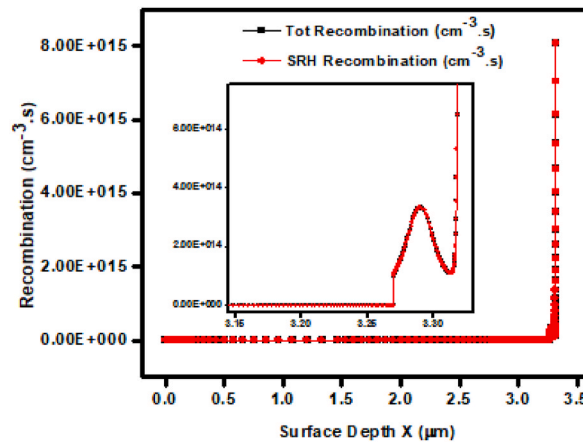


Fig. 9. Recombination rates versus diffusion length of optimized solar cell.

of charge carrier recombination with depth within the composition of the perovskite solar cell. As the light enters the surface, zero recombination of charge carriers is observed up to a depth value of 3.27 μm . A significant increase in carrier recombination is then observed from 3.27 μm to 3.33 μm . Interestingly, it is noted that the trap assisted recombination and total recombination remain relatively constant throughout the diffusion length, peaking at $8.00 \times 10^{15} \text{ cm}^{-3} \text{ s}$ at 3.35 μm . This observation highlights the importance of understanding recombination mechanisms in the design and optimization of perovskite solar cells.

3.2. Effects of variation of SnO_2 electron transport layer thickness

The electron transport layer (ETL) holds a pivotal role in perovskite solar cells. It is responsible for collecting and transporting the electrons generated by the perovskite absorber layer to the external circuit. Additionally, the ETL helps to block holes from the hole transport layer (HTL) and prevent recombination of the electrons and holes. Moreover, the ETL optimize the energy level alignment between the perovskite absorber and the electrode, which is crucial for achieving high open-circuit voltage (V_{oc}) and power conversion

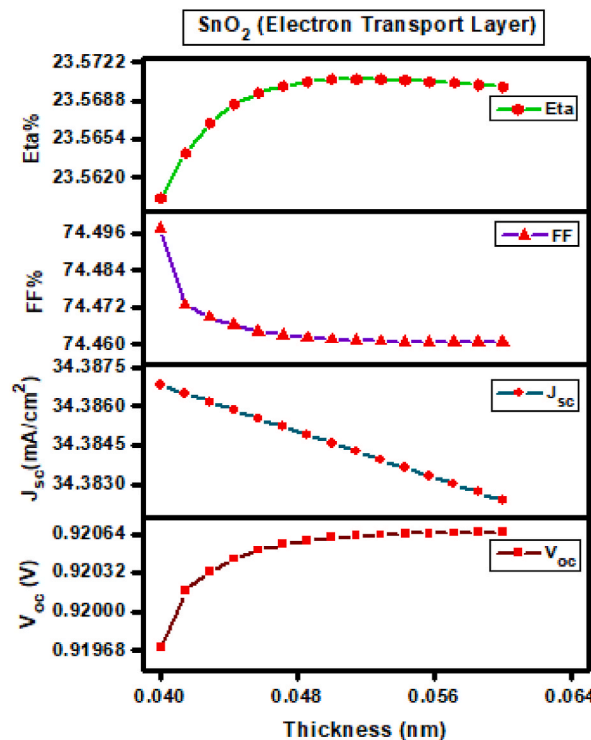


Fig. 10. Electrical parameters (V_{oc} , J_{sc} , FF, PCE) versus thickness for SnO_2 -ETL.

efficiency (PCE). The choice of ETL material, its thickness, and surface properties can significantly impact the device performance. SCAPS-1D was employed to investigate the impact of the depth of the electron transport layer (SnO_2) on the electrical parameters of the perovskite solar cell, including V_{oc} , J_{sc} , FF, and PCE. The thickness of the SnO_2 layer was systematically varied from 0.040 nm to 0.060 nm while keeping the thickness of the CuSCN and $\text{CH}_3\text{NH}_3\text{SnI}_3$ perovskite layer constant. The results showed that the highest PCE was obtained at an optimized SnO_2 layer thickness of 0.05 nm. At this thickness, the peak values of V_{oc} , J_{sc} , FF, and PCE were 0.92 V, 34.38 mA/cm^2 , 74.46 %, and 23.57 %, respectively, indicating a significant improvement in the device output. Interestingly, the electrical parameters were found to remain unaffected by changes in the electron transport layer (ETL) thickness. This can be attributed to the fact that the generation of charge carriers is primarily assisted by the $\text{CH}_3\text{NH}_3\text{SnI}_3$ perovskite absorber layer, while the ETL only serves to transport the charges. The electrical parameters corresponding to possible variations in the SnO_2 (ETL) thickness are presented in figure-10.

3.3. Effects of variation of $\text{CH}_3\text{NH}_3\text{SnI}_3$ absorber materials thickness

The $\text{CH}_3\text{NH}_3\text{SnI}_3$ (methylammonium tin iodide) absorber layer is a key component of perovskite solar cells, playing a critical role in optimizing their performance. When light enters the cell, the perovskite absorber layer absorbs it, generating charge carriers (electrons and holes). These carriers are then transported through the cell and collected at the respective electrodes to produce an electrical current. The unique properties of $\text{CH}_3\text{NH}_3\text{SnI}_3$ make it an excellent absorber material for solar cells. It possesses a high absorption coefficient, efficiently absorbing light across a broad range of the solar spectrum. Furthermore, it has high carrier mobility, allowing charge carriers to move quickly and easily through the material. This is crucial for minimizing losses due to recombination of the carriers within the device. Moreover, the $\text{CH}_3\text{NH}_3\text{SnI}_3$ perovskite material is easily synthesized through low-temperature solution processing techniques, enabling low-cost and scalable fabrication of solar cells.

In summary, the $\text{CH}_3\text{NH}_3\text{SnI}_3$ absorber layer is critical to the performance of perovskite solar cells, as it efficiently absorbs light, generates charge carriers, and facilitates charge carrier transport. SCAPS-1D was utilized to investigate the impact of the thickness of the absorber layer ($\text{CH}_3\text{NH}_3\text{SnI}_3$) on the key electrical parameters, namely V_{oc} , J_{sc} , FF, and PCE, in a perovskite solar cell. The thickness of the $\text{CH}_3\text{NH}_3\text{SnI}_3$ layer was varied from 2.70 μm to 3.30 μm , while keeping the thicknesses of the CuSCN and SnO_2 layers constant. The optimized thickness for the absorber layer was found to be 3.2 μm , which resulted in the highest power conversion efficiency. The peak values of V_{oc} , J_{sc} , FF, and PCE were 0.92 V, 34.39 mA/cm^2 , 74.46%, and 23.57%, respectively, at this optimized thickness. The increase in current density with an increase in the thickness of the $\text{CH}_3\text{NH}_3\text{SnI}_3$ light harvesting layer leads to an overall increase in device efficiency. Additionally, exposing the absorber layer to sunlight results in a greater number of electrons and holes being generated, enhancing electron mobility. However, the reduction in fill factor (FF) is observed due to recombination and a reduction in the lifetime of charge carriers within the absorber layer. Figure-11 shows the electrical parameters corresponding to variations in the

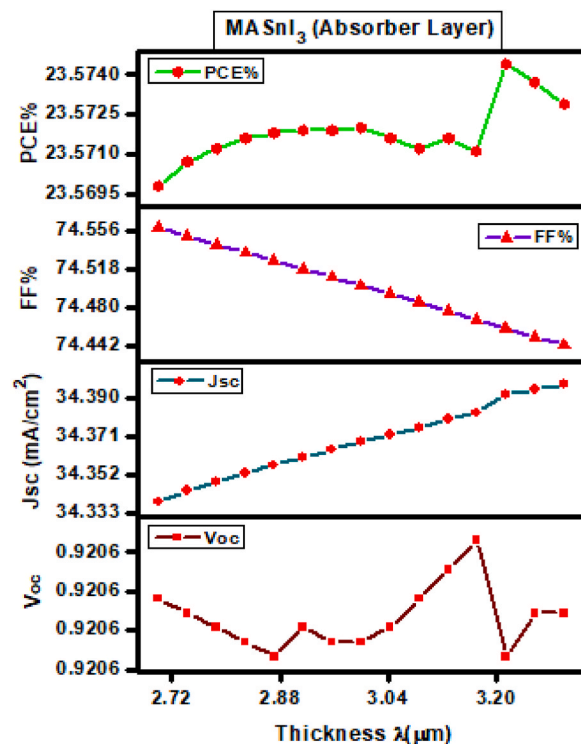


Fig. 11. Electrical parameters (V_{oc} , J_{sc} , FF, PCE) versus thickness for $\text{CH}_3\text{NH}_3\text{SnI}_3$ absorber.

thickness of the absorber layer ($\text{CH}_3\text{NH}_3\text{SnI}_3$).

3.4. Effects of variation of CuSCN-HTL thickness

In a solar cell, the role of HTL is to transport the holes generated by the absorption of light in the active layer to the electrode. The HTL is typically located between the active layer and the top electrode. The HTL is important for achieving high efficiency in the solar cell because it needs to efficiently transport holes while blocking the transport of electrons. This mechanism aids in preventing charge recombination and enhancing the overall efficiency of the device. The performance of the HTL can be optimized by varying its thickness, composition, and morphology. The thickness of the HTL can influence device performance by changing series resistance and increasing the recombination rate. Moreover, the choice of HTL material can have a significant impact on device performance, as certain materials offer superior conductivity and stability compared to others. Using SCAPS-1D, the impact of the thickness of the HTL CuSCN (copper thiocyanate) on the electrical parameters (V_{oc} , J_{sc} , FF, and PCE) was analyzed. The CuSCN layer was varied from 0.05 μm to 0.08 μm , while keeping the thickness of the $\text{CH}_3\text{NH}_3\text{SnI}_3$ and SnO_2 layers constant. The highest PCE was observed for an optimized CuSCN layer thickness of 0.07 μm . At this thickness, the peak values of V_{oc} , J_{sc} , FF, and PCE were found to be 0.92 V, 34.38 mA/cm^2 , 74.45%, and 23.56%, respectively, as illustrated in figure-12.

3.5. Effects of variation in temperature on optimized solar cell

Temperature plays a crucial role in optimizing the performance of a solar cell. The efficiency of a solar cell is affected by the amount of energy that can be extracted from the incident light, and the temperature of the solar cell affects the ability to extract this energy.

At low temperatures, the efficiency of a solar cell is limited due to a lack of energy to produce charge carriers. As the temperature increases, the generation of charge carriers also increases, leading to an increase in the overall efficiency of the solar cell. However, if the temperature becomes excessively high, the performance of the solar cell can be constrained due to an increase in the number of recombination events that occur within the device, subsequently decreasing the overall efficiency. Temperature plays a significant role in analyzing the output of the device due to its dependence on the electrical parameters, as illustrated in figure-13. As the temperature rises, the short circuit current density (J_{sc}) corresponding to the augmentation increases, reaching a maximum of 34.39 mA/cm^2 at 340 K. This is attributed to an increase in the creation of charge carriers. However, initially, from 300 K to 305 K, the abrupt creation of charge carriers leads to collisions and phonon movements, resulting in a decrease in the value of the Fill Factor (FF). The increasing trend of J_{sc} is caused by a greater number of lattice expansions and attenuation occurring among atoms within bonds.

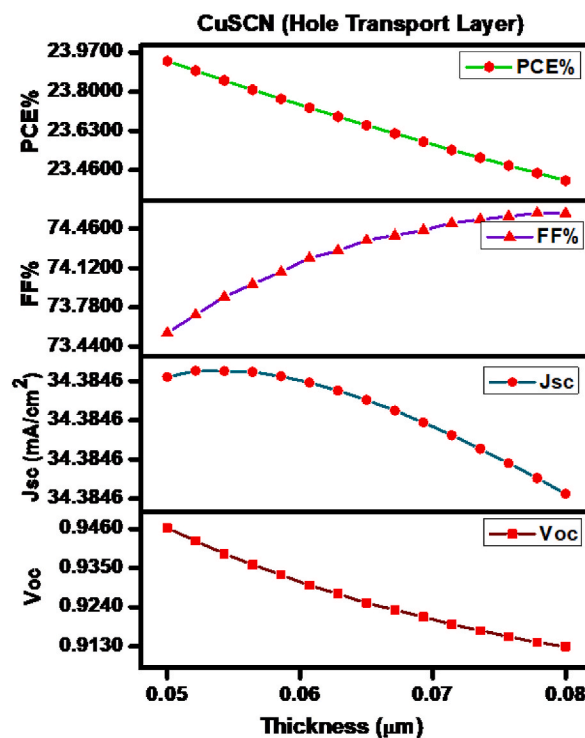


Fig. 12. Electrical parameters (V_{oc} , J_{sc} , FF, PCE) versus thickness for CuSCN-HTL.

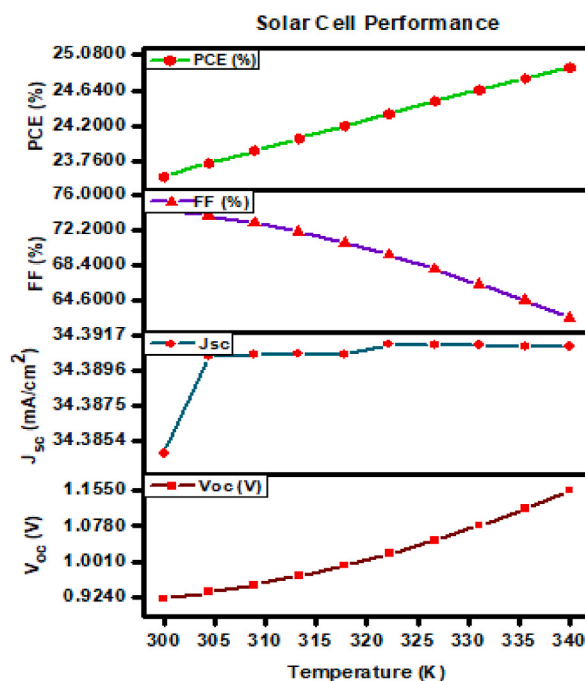


Fig. 13. Electrical parameters versus Temperature for optimized solar cell.

3.6. Optimized performance of proposed solar module using PVSyst

The IV characteristics of a solar module composed of 72 solar cells ($\text{SnO}_2\text{-}/\text{CH}_3\text{NH}_3\text{SnI}_3/\text{CuSCN}$) were simulated using input parameters obtained from SCAPS 1D and entered into PVSyst simulation software. The calculations were conducted at a fixed temperature of 45 °C for five distinct irradiation intensities intervals in 200–1000 W/m^2 . The results, depicted in figure-14, indicate that an increase in irradiation intensity corresponds to a rise in the current generated by the solar module. This increase can be attributed to the increase in the number of photons absorbed by the solar cells, which leads to a higher number of electron-hole pairs being generated. The increase in current was observed in all five curves, with the highest current observed at the highest irradiation intensity of 1000 W per square meter. In addition to the increase in current, the IV curves show a slight rise in voltage with increasing irradiation intensity. This is because the resistance of the solar cells decreases at higher irradiation intensities. The simulated IV characteristics provide valuable information for optimizing the performance of the solar module under various operating conditions. This information can be utilized to optimize the design and configuration of the solar module and forecast its energy output under diverse operating conditions. In summary, the IV characteristics of the solar module indicate that it is capable of generating higher currents at higher irradiation intensities, which is crucial for enhancing the performance of solar modules in real-world applications.

The IV characteristics of a solar module, consisting of 72 solar cells based on $\text{SnO}_2\text{-}/\text{CH}_3\text{NH}_3\text{SnI}_3/\text{CuSCN}$ composition of solar cells, were simulated using PVSyst simulation software. The simulations were conducted at a fixed irradiation intensity of 1000 W/m^2 and at different temperatures ranging from 10 to 70 °C. The results revealed that with an increase in temperature, there was a corresponding decrease in the maximum power obtained from the solar module. The maximum power obtained was 557.4 W at 10 °C, 546.1 W at 25 °C, 534.6 W at 40 °C, 522.9 W at 55 °C, and 510.9 W at 70 °C. These values are plotted in figure-15, with detailed power output information provided in the inset. The decline in the maximum power output can be attributed to the decrease in the efficiency of the solar cells as temperature increases. At higher temperatures, the mobility of charge carriers decreases, which leads to a decrease in the current generated by the solar cells. Additionally, there is an increase in the recombination rate of electron-hole pairs at higher temperatures, further contributing to the decrease in the maximum power output. The IV curves also exhibited that the voltage and current output decreased with increasing temperature. This decrease is due to the increase in the resistance of the solar cells at higher temperatures, which reduces the amount of power that can be extracted from the solar module. Consequently, the IV characteristics of the $\text{SnO}_2\text{-}/\text{CH}_3\text{NH}_3\text{SnI}_3/\text{CuSCN}$ -based solar module demonstrated that the maximum power output decreased with increasing temperature. This information can be used to optimize the performance of the solar module under different operating conditions, including temperature, and forecast the energy output of the solar module under diverse operating conditions.

The PV characteristics of a solar module, comprising 72 solar cells ($\text{SnO}_2\text{-}/\text{CH}_3\text{NH}_3\text{SnI}_3/\text{CuSCN}$), were studied using PVSyst simulation software as given in figure-16. Input parameters were obtained from SCAPS 1D and utilized for the simulations. The module was exposed to five different irradiation intensities ranging from 200 to 1000 W per square meter, while maintaining a constant temperature of 45 °C. The results demonstrated a direct correlation between the incident irradiation intensity and the power output of the solar module. As the irradiation intensity increased, the power output also increased. The five curves obtained at the different irradiation intensities demonstrated a rise in the power output, with values of 108.3 W, 218.4 W, 325.6 W, 429.8 W, and 530.7 W

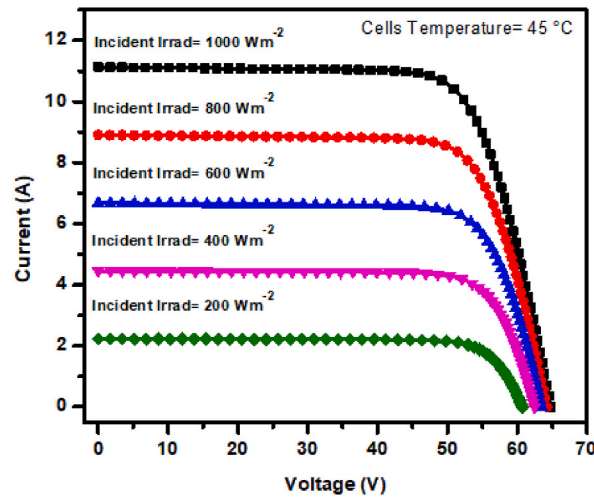


Fig. 14. IV Characteristics of solar module based on (SnO₂/CH₃NH₃SnI₃/CuSCN) solar cell at different incident irradiation intensities.

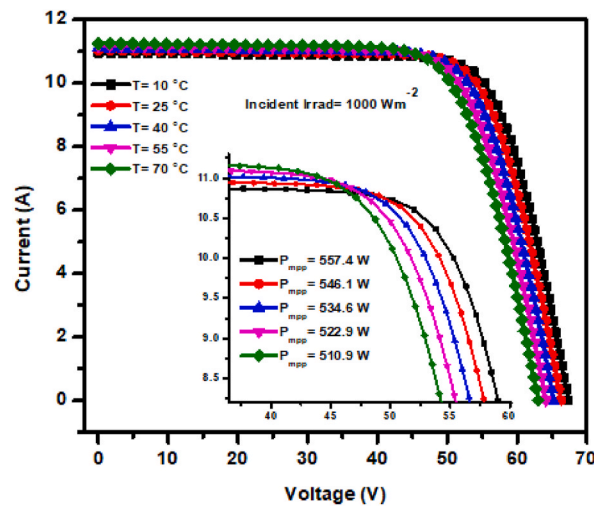


Fig. 15. IV Characteristics of solar module based on (SnO₂/CH₃NH₃SnI₃/CuSCN) solar cell at different temperatures.

obtained at 200, 400, 600, 800, and 1000 W per square meter irradiation intensities, respectively. The study reveals that there is a positive relationship between the incident irradiation intensity and the power output of the SnO₂/CH₃NH₃SnI₃/CuSCN-based solar module. These findings can be utilized to optimize the performance of the solar module and predict its energy output under various operating conditions.

The PV characteristics of a solar module, comprising of 72 solar cells based on SnO₂/CH₃NH₃SnI₃/CuSCN, were simulated using PVSystem simulation software. The simulations were carried out at a fixed incident irradiation of 1000 W per square meter and at temperatures ranging from 10 to 70 °C, generating five curves for each temperature as shown in figure-17. The results reveal that with an increase in temperature, there is a corresponding decrease in the maximum power output of the solar module. The maximum power obtained was 557.4 W at 10 °C, 546.1 W at 25 °C, 534.6 W at 40 °C, 522.9 W at 55 °C, and 510.9 W at 70 °C. This decrease in maximum power output can be attributed to the decrease in the efficiency of the solar cells at higher temperatures. The decrease in efficiency is due to many factors. Firstly, as the temperature increases, the mobility of charge carriers decreases, resulting in a reduction in the current generated by the solar cells. Additionally, at higher temperatures, there is an increase in the recombination rate of electron-hole pairs, further contributing to the decrease in the maximum power output. The PV curves also showed that both the voltage and current output decreased with increasing temperature. This decrease is due to the increase in the resistance of the solar cells at higher temperatures, reducing the amount of power that can be extracted from the solar module. In summary, The PV characteristics of SnO₂/CH₃NH₃SnI₃/CuSCN -based solar module demonstrated a reduction in maximum power output with increasing temperature. This information can be useful for optimizing the performance of the solar module under different operating conditions and predicting its energy output under varying environmental conditions.

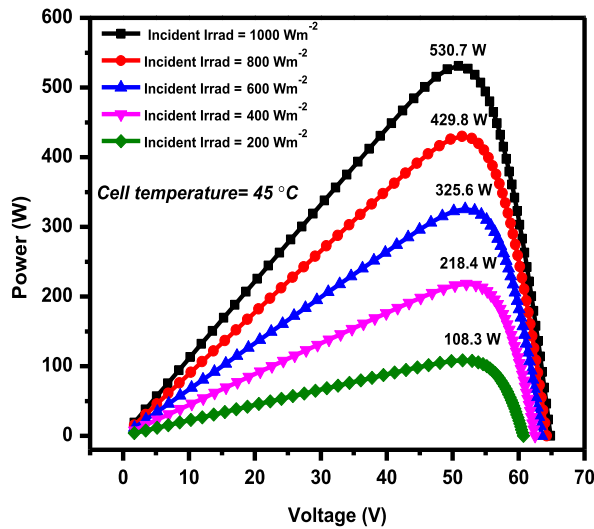


Fig. 16. PV Characteristics of solar module based on (SnO₂/CH₃NH₃SnI₃/CuSCN) solar cell at different incident irradiation intensities.

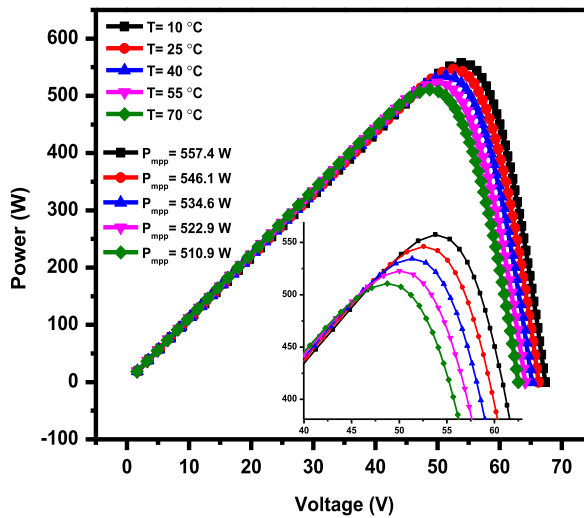


Fig. 17. IV Characteristics of solar module based on (SnO₂/CH₃NH₃SnI₃/CuSCN) solar cell at different temperatures.

The performance ratio (PR) of a solar energy system for each month of the year is shown in figure-18. The performance ratio is defined as the ratio of the actual energy output of the system to the expected energy output based on the available solar radiation. The PR values for each month are as follows: Jan 0.8255, Feb 0.8224, Mar 0.8324, Apr 0.7499, May 0.826, Jun 0.7639, Jul 0.8206, Aug 0.8204, Sep 0.8268, Oct 0.7409, Nov 0.8269, and Dec 0.8181. From the results, it may be observed that the PR values fluctuate throughout the year, reaching the highest value in March and the lowest value in April. This suggests that the solar energy system is most efficient in March when the available solar radiation is at its peak and least efficient in April when the solar radiation is lower. The PR values also show some variation during the summer, with the lowest value in June and the highest value in September. This variation could be attributed to fluctuations in weather conditions or other factors impacting the performance of the solar energy system. The PR values for the solar energy system remain relatively stable throughout the year, with only minor fluctuations. This indicates that the system operates consistently and reliably, performing well in various weather conditions and seasonal variations.

The data provided in the table-1 illustrates the monthly and annual energy output of a PV system along with some environmental parameters [32]. The data also indicates that the PR of the system was highest in March and September, implying that the system was most efficient during these months. The calculated data can be useful in optimizing the design and performance of PV systems to enhance their efficiency and reduce the cost of solar energy production.

The horizon profile diagram presented in figure-19 is a tool utilized in PVsyst software to assess shading of a PV array caused by objects in the surrounding environment, such as buildings, trees, or hills. The diagram displays the silhouette of these objects on a vertical plane, providing a visual representation of the potential shading impact on the PV system. In the horizon profile diagram, the

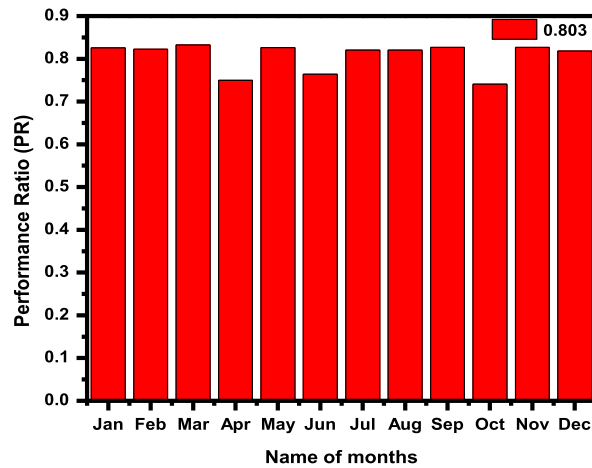


Fig. 18. Annual performance ration of solar module based on (SnO₂/CH₃NH₃SnI₃/CuSCN) perovskite solar cell.

Table-1

Months	GlobHor kWh/m ²	DiffHor kWh/m ²	T_Amb °C	GlobInc kWh/m ²	GlobEff kWh/m ²	EArray kWh	E_Grid kWh	PR ratio
January	82.8	33.98	9.88	105.4	97.8	52569	51136	0.825
February	83.4	51.03	13.13	97.6	91	48505	47193	0.822
March	140.6	65.32	18.86	172.6	162.6	86647	84471	0.832
April	165.5	78.51	23.94	201.3	190.7	100978	88753	0.75
May	204	86.18	29.8	250.7	238.6	124977	121764	0.826
June	195.9	99.25	31.01	231.5	219.6	114482	103985	0.764
July	183.3	96.82	30.25	216.1	204.9	106985	104263	0.821
August	168.3	95.66	28.98	197.1	186.2	97488	95052	0.82
September	163.6	64.93	26.71	205.2	194.1	102310	99738	0.827
October	144	47.15	22.46	185	174.3	92411	80577	0.741
November	108.2	30.57	15.65	142	132.2	70745	69018	0.827
December	79.2	32.03	11.39	100.8	93.1	49845	48463	0.818
Year	1718.9	781.42	21.88	2105.1	1985	1047942	994414	0.803

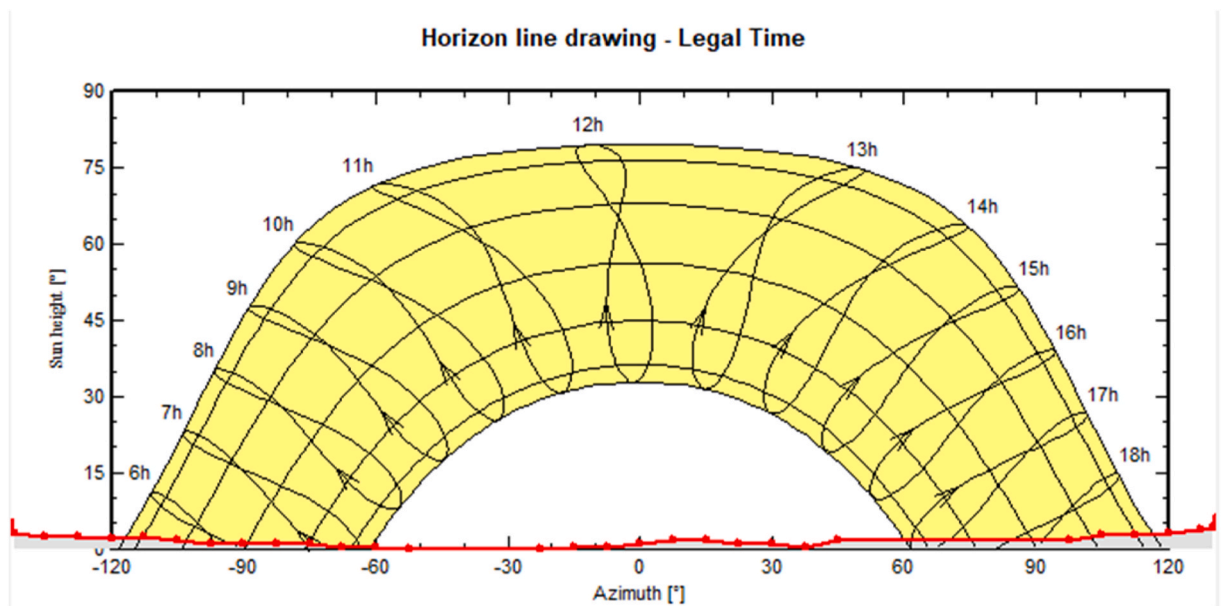


Fig. 19. Horizon profile for (SnO₂/CH₃NH₃SnI₃/CuSCN) based solar module.

horizontal axis represents the azimuth angle in degrees, while the vertical axis represents the altitude angle in degrees. The altitude angle measures the elevation of the sun above the horizon, while the azimuth angle measures the angle between the sun's position and true north. The silhouette of the surrounding objects is plotted on the horizon profile diagram, with the highest point of the object located at the altitude angle corresponding to its height above the PV system. Moreover, the diagram also illustrates the sun's path throughout the day, with each point on the path representing the sun's position at a specific time. Analyzing the horizon profile diagram enables the identification of potential shading sources and evaluation of the shading's impact on the PV system. The shading analysis can be used to optimize the placement and orientation of the PV array, as well as to design appropriate shading mitigation strategies. The horizon profile diagram is an important tool for assessing shading in a PV system and optimizing its performance, particularly in areas with complex terrain or urban environments where shading can significantly impact energy production.

4. Conclusions

In our research, we critically optimized and analyzed the ITO/SnO₂/CH₃NH₃SnI₃/CuSCN/Mo perovskite-based solar cell composition. Our objective was to achieve an enhanced power conversion efficiency (PCE) and short circuit current density (J_{sc}) using solar capacitance simulator. We observed that variations in the layer thickness of the CH₃NH₃SnI₃ (Perovskite Absorber Layer), SnO₂ (ETL), and CuSCN (HTL) have a significant impact on the corresponding electrical parameters. Optimized values of 0.05 nm for SnO₂, 0.07 μ m for CuSCN, and 3.2 μ m for CH₃NH₃SnI₃ produced an encouraging PCE of 23.57%, J_{sc} of 34.38 mA/cm², open circuit voltage (V_{oc}) of 0.9260V, and Fill Factor (FF) of 74.46%, respectively. The PCE associated with the CH₃NH₃SnI₃-absorber is strongly influenced by the enhancement of hole and electron mobilities. However, it is more important to consider low electron carrier recombination, especially in relation to high electron carrier mobility. The tuning of the band-gap associated with each incorporated layer, maximizing device output, signifies an enhancement in the PCE with associated band-gap values of 3.4eV for CuSCN, 1.35eV for CH₃NH₃SnI₃-light harvester, and 3.6eV for SnO₂. This effect may be attributed to stronger recombination of charge carriers, particularly at interfaces. An increase in surface depth raised the recombination rate of associated charge carriers, thus reducing the overall performance. Notably, the device exhibited optimal efficiency at temperatures between 335K and 340K. Based on the simulated results in SCAPS-1D, the input parameters incorporated in PVSyst software package demonstrated an impressive output, resulting in a power creation of 557.4 W for a module consisting of 72 cells with annual performance ratio of 80.3 %. There is a significant need to emphasize the search for more suitable compositions like the proposed one, to explore even more efficient results in terms of PCE, with reduced recombination rates and cost-effectiveness.

Data availability statement

We hereby submit our manuscript entitled "Development of Low-Cost and High-Efficiency Solar Modules Based on Perovskite Solar Cells for Large-Scale Applications". The data utilized in this article has not been previously submitted in any repository. To ensure transparency and facilitate further research, the data may be made available for academic and research purposes by emailing the corresponding author *Dr. Irfan Qasim* at email ID: dr.irfanqasim@gmail.com.

CRediT authorship contribution statement

Muhammad Shoaib Hanif: Writing – original draft, Investigation. **Irfan Qasim:** Writing – review & editing, Formal analysis, Conceptualization. **Muhammad Imran Malik:** Software, Data curation. **Muhammad Farooq Nasir:** Writing – review & editing, Methodology, Investigation. **Owais Ahmad:** Writing – review & editing, Software. **Asim Rashid:** Formal analysis, Software, Validation.

Declaration of competing interest

The authors declare that they have no known competing financial interests or personal relationships that could have appeared to influence the work reported in this paper.

Acknowledgments

The authors express their gratitude to Dr. Marc Burgelman and his team at the Electronics and Information Systems (ELIS) Laboratory, University of Ghent, Belgium for providing access to the SCAPS-1D software. They also extend their appreciation to A. Mermoud and M. Viloz at Geneva University, Switzerland for the PVSyst solar module simulation software.

References

- [1] Prasanth K. Enaganti, et al., Study of solar irradiance and performance analysis of submerged monocrystalline and polycrystalline solar cells, Prog. Photovoltaics Res. Appl. 28 (7) (2020) 725–735, <https://doi.org/10.1002/pip.3264>.
- [2] J. Liu, K. Chen, S.A. Khan, B. Shabbir, Y. Zhang, Q. Khan, Q. Bao, Nanotechnology 31 (15) (2020) 152002, <https://doi.org/10.1088/1361-6528/ab5a19>. PMID: 31751979.
- [3] T. Kim, J. Lim, S. Song, Recent progress and challenges of electron transport layers in organic–inorganic perovskite solar cells, Energies 13 (21) (2020) 5572, <https://doi.org/10.3390/en13215572>.

- [4] J. Liu, B. Shabbir, C. Wang, T. Wan, Q. Ou, P. Yu, Q. Bao, Flexible, printable soft-X-ray detectors based on all-inorganic perovskite quantum dots, *Adv. Mater.* 31 (30) (2019) 1901644, <https://doi.org/10.1002/adma.201901644>.
- [5] J. Liu, B. Shabbir, C. Wang, T. Wan, Q. Ou, P. Yu, A. Tadich, X. Jiao, D. Chu, D. Qi, D. Li, R. Kan, Y. Huang, Y. Dong, J. Jasieniak, Y. Zhang, Q. Bao, *Adv. Mater.* 31 (30) (2019) 1901644, <https://doi.org/10.1002/adma.201901644>.
- [6] H.A. Jame, S. Sarker, M.S. Islam, M.T. Islam, A. Rauf, S. Ahsan, S. Ahmed, Supervised machine learning-aided SCAPS-based quantitative analysis for the discovery of optimum bromine doping in methylammonium tin-based perovskite (MASnI_{3-x}Br_x), *ACS Appl. Mater. Interfaces* (2021), <https://doi.org/10.1021/acsami.1c15030>.
- [7] A. Younis, L. Hu, P. Sharma, C.H. Lin, Y. Mi, X. Guan, D. Zhang, Y. Wang, T. He, X. Liu, B. Shabbir, S. Huang, J. Seidel, T. Wu, *Adv. Funct. Mater.* 30 (31) (2020) 2002948, <https://doi.org/10.1002/adfm.202002948>.
- [8] M.I. Ahmed, A. Habib, S.S. Javaid, Perovskite solar cells: potentials, challenges, and opportunities (2015), *Int. J. Photoenergy* (2015).
- [9] L. Qiu, L.K. Ono, Y. Qi, Advances and challenges to the commercialization of organic-inorganic halide perovskite solar cell technology, *Mater. Today Energy* 7 (2018) 169–189, <https://doi.org/10.1016/j.mtener.2017.09.008>.
- [10] F. Giustino, H.J. Snaith, Toward lead-free perovskite solar cells, *ACS Energy Lett.* 1 (6) (2016) 1233–1240, <https://doi.org/10.1021/acsenergylett.6b00499>.
- [11] Y. Zheng, R. Su, Z. Xu, D. Luo, H. Dong, B. Jiao, R. Zhu, Perovskite solar cell towards lower toxicity: a theoretical study of physical lead reduction strategy, *Sci. Bull.* 64 (17) (2019) 1255–1261, <https://doi.org/10.1016/j.scib.2019.06.006>.
- [12] G. Schileo, G. Grancini, Lead or no lead? Availability, toxicity, sustainability and environmental impact of lead-free perovskite solar cells, *J. Mater. Chem. C* 9 (1) (2021) 67–76, <https://doi.org/10.1039/D0TC04552G>.
- [13] NREL, Cell-efficiency.html. <https://www.nrel.gov/pv/cell-efficiency.html>, 2020. (Accessed 10 April 2020). <https://pvdpc.nrel.gov/>.
- [14] Qingdong Lin, Stefano Bernardi, Babar Shabbir, Qingdong Ou, Mingchao Wang, Wenping Yin, Shiqi Liu, Anthony S. R. Chesman, Sebastian O. Furer, Guangyuan Si, Nikhil Medhekar, Jacek Jasieniak, Asaph Widmer-Cooper, Wenxin Mao, Udo Bach, *Advanced Functional Materials*, Volume32, Issue16, April 19, 2022, 2109442. <https://doi.org/10.1002/adfm.202109442>.
- [15] R. Vidal, J.A. Alberola-Borras, N. Sanchez-Pantoja, I. Mora-Sero, Comparison of perovskite solar cells with other photovoltaics technologies from the point of view of life cycle assessment, *Advanced Energy and Sustainability Research* 2 (5) (2021) 2000088, <https://doi.org/10.1002/aesr.202000088>.
- [16] Mohammad I. Hossain, Fahhad H. Alharbi, Nouar Tabet, Copper oxide as inorganic hole transport material for lead halide perovskite based solar cells, *Sol. Energy* 120 (2015) 370–380, <https://doi.org/10.1016/j.solener.2015.07.040>.
- [17] F.M. Rombach, S.A. Haque, T.J. Macdonald, Lessons learned from spiro-OMeTAD and PTAA in perovskite solar cells, *Energy Environ. Sci.* (2021), <https://doi.org/10.1039/D1EE02095A>.
- [18] C.J. Yu, Advances in modelling and simulation of halide perovskites for solar cell applications, *J. Phys.: Energy* 1 (2) (2019) 022001, <https://doi.org/10.1088/2515-7655/aaf143>.
- [19] Hui-Jing Du, Wei-Chao Wang, Jian-Zhuo Zhu, Device simulation of lead-free CH₃NH₃SnI₃ perovskite solar cells with high efficiency, *Chin. Phys. B* 25 (10) (2016) 108802, <https://doi.org/10.1088/1674-1056/25/10/108802>.
- [20] Z. Dai, Q. Ou, C. Wang, G. Si, B. Shabbir, C. Zheng, Z. Wang, Y. Zhang, Y. Huang, Y. Dong, J. Jasieniak, B. Su, Q. Bao, *J. Mater. Chem. C* 7 (2019) 5954–5961, <https://doi.org/10.1039/C9TC01104H>.
- [21] Babar Shabbir, Jingying Liu, Vaishnavi Krishnamurthi, R.A.W. Ayyubi, Kevin Tran, Sherif Abdulkader Tawfik, M. Mosarof Hossain, Hareem Khan, Yingjie Wu, Bannur Nanjunda Shivananju, Rizwan Ur Rehman Sagar, Asif Mahmood, Adnan Younis, Md Hemayet Uddin, Syed A. Bukhari, Sumeet Walia, Yongxiang Li, Michelle J.S. Spencer, Nasir Mahmood, Jacek J. Jasieniak, January, *Advanced Functional Materials*, Volume32, Issue3, Special Issue: Focus Issue on the Australian National Fabrication Facility 14 (2022) 2105038, <https://doi.org/10.1002/adfm.202105038>.
- [22] L. Huang, X. Sun, C. Li, R. Xu, J. Xu, Y. Du, J. Zhang, Electron transport layer-free planar perovskite solar cells: further performance enhancement perspective from device simulation, *Sol. Energy Mater. Sol. Cell.* 157 (2016) 1038–1047, <https://doi.org/10.1016/j.solmat.2016.08.025>.
- [23] B. Shabbir, M. Nadeem, Z. Dai, M.S. Fuhrer, Q.K. Xue, X. Wang, Q. Bao, *Appl. Phys. Rev.* 5 (2018) 041105, <https://doi.org/10.1063/1.5040694>.
- [24] Owais Ahmad, Irfan Qasim, Syed M. Hasnain, Zain ul Abidin, Muhammad Farooq Nasir, Muhammad Imran Malik, Asim Rashid, “Modelling and numerical simulations of eco-friendly double absorber solar cell “Spiro-OmeTAD/CIGS/MASnI₃/CdS/ZnO” and its PV-module” *Organic, Electronics* 117 (2023) 106781, <https://doi.org/10.1016/j.orgel.2023.106781>.
- [25] M.S. Chowdhury, S.A. Shahahmadi, P. Chelvanathan, S.K. Tiong, N. Amin, K.A. Techato, M. Suklueng, Effect of deep-level defect density of the absorber layer and n/i interface in perovskite solar cells by SCAPS-1D, *Results Phys.* 16 (2020) 102839, <https://doi.org/10.1016/j.rinp.2019.102839>.
- [26] F. Izadi, A. Ghobadi, A. Gharaati, M. Minbashi, A. Hajjiah, Effect of interface defects on high efficient perovskite solar cells, *Optik* 227 (2021) 166061, <https://doi.org/10.1016/j.jlleo.2020.166061>.
- [27] M.S. Jamal, S.A. Shahahmadi, M.A.A. Wadi, P. Chelvanathan, N. Asim, H. Misran, M. Akhtaruzzaman, Effect of defect density and energy level mismatch on the performance of perovskite solar cells by numerical simulation, *Optik* 182 (2019) 1204–1210, <https://doi.org/10.1016/j.jlleo.2018.12.163>.
- [28] Usha Mandadapu, et al., Design and simulation of high efficiency tin halide perovskite solar cell, *Int. J. Renew. Energy Res* 7 (2017) 4, <https://doi.org/10.20508/ijrer.v7i4.6182.g7270>.
- [29] Y. Gan, X. Bi, Y. Liu, B. Qin, Q. Li, Q. Jiang, P. Mo, Numerical investigation energy conversion performance of tin-based perovskite solar cells using cell capacitance simulator, *Energies* 13 (22) (2020) 5907, <https://doi.org/10.3390/en13225907>.
- [30] K.D. Jayan, V. Sebastian, Comprehensive device modelling and performance analysis of MASnI₃ based perovskite solar cells with diverse ETM, HTM and back metal contacts, *Sol. Energy* 217 (2021) 40–48, <https://doi.org/10.1016/j.solener.2021.01.058>.
- [31] H. Zhang, X. Ji, H. Yao, Q. Fan, B. Yu, J. Li, Review on efficiency improvement effort of perovskite solar cell, *Sol. Energy* 233 (2022) 421–434, <https://doi.org/10.1016/j.solener.2022.01.060>.
- [32] Irfan Qasim, Muhammad Imran Malik, Simulations and suitability study of inorganic Cu-based hole-transport layers in planar CH₃NH₃SnI₃-based perovskite solar cell and module, *Energy Technol.* (2023) 2300471, <https://doi.org/10.1002/ente.202300471>.